Photodissociation of HCl and DCl: Polarization of Atomic Photofragments†

Alex Brown*

Department of Chemistry, University of Alberta, Edmonton, AB, T6G 2G2, Canada

G. G. Balint-Kurti‡

School of Chemistry, University of Bristol, Bristol BS8 1TS, United Kingdom

O. S. Vasyutinskii

Ioffe Physico-Technical Institute, Russian Academy of Sciences, 194021 St. Petersburg, Russia

Received: January 16, 2004; In Final Form: March 4, 2004

The complete angular momentum distributions and vector correlation coefficients (orientation and alignment) of ground-state Cl($^2P_{3/2}$) and excited-state Cl($^2P_{1/2}$) atoms resulting from the photodissociation of HCl have been computed as a function of photolysis energy. Results for the corresponding H atom partner are also calculated and demonstrate that the H-atom produced is highly spin polarized. The theoretical results are determined using a time-dependent wave packet treatment of the dissociation dynamics based on ab initio potential energy curves, spin−orbit couplings, and dipole moments that have been reported previously [Alexander, M. H.; Pouilly, B.; Duhoo, T. *J. Chem. Phys.* **1993**, *99*, 1752]. The theoretical orientation and alignment parameters, $\mathbf{a}_Q^{(K)}(p)$, that describe the coherent and incoherent contributions to the angular momentum distributions from the multiple dissociative states accessed by parallel and perpendicular transitions, are compared to experimental measurements made at 193 nm and excellent agreement is obtained. Theoretical predictions of the $\mathbf{a}_Q^{(K)}(p)$ parameters for the isotopically substituted species DCl, for which no experiments have yet been carried out, are reported and contrasted to the analogous HCl results. The results for the H atom spin polarizations are discussed in the context of three static models whose strengths and limitations are highlighted.

1. Introduction

Molecular photofragmentation is often interpreted assuming that the dissociation takes place only on a single adiabatic electronic state. However, in general, multiple (coupled) dissociative states are often involved in the dissociation process. More important, nonadiabatic transitions between these states may occur as the molecule dissociates. Additionally, there can be quantum mechanical interference between these multiple dissociative pathways. Our understanding of the dissociation dynamics, especially as it pertains to evolution on multiple electronic states, requires both high-level theoretical calculations and the accurate experimental measurement of a variety of observables, particularly angular momentum distributions.

In general, the photodissociation of a diatomic molecule AB yields open-shell fragments A and B. The resulting photofragments, possessing angular momenta j_A and j_B, respectively, can have a preferred orientation in space. If j_A and j_B include a contribution from electron orbital angular momenta, this preferred orientation is associated with an anisotropic electron distribution about a body-fixed *z*-axis (which, of course, implies an anisotropic electron distribution about any chosen space-fixed *Z*-axis). A mechanism for photofragment electronic polarization was first proposed by Van Brunt and Zare[1] and the first experiments investigating the angular distribution of photofragments arising from the photodissociation process were performed by Bersohn.[2,3] More recently, Siebbles et al.[4] have shown that the spatial distribution of the photofragment angular momenta can be decomposed into distinct contributions from dissociation on a single potential energy surface (PES) and from the interference from dissociation through multiple PESs. For a fragment with angular momentum j, the magnitude of these distinct spatial distributions (in the molecular frame) can be fully described by the $\mathbf{a}_Q^{(K)}(p)$ parameters,[5,6] where K and Q refer to the spatial distributions in the molecular frame and p refers to the symmetry of the transition dipole moment from the ground electronic state to the dissociating state. The symmetry *p* can be ⊥, ||, or (||, ⊥) corresponding to pure perpendicular, pure parallel, or mixed parallel/perpendicular excitation. Note that an alternate set of anisotropy parameters[7,8] related to the laboratory frame has also been introduced. In concert with the phenomenological advances in describing the angular distributions of atomic photofragments, sophisticated experimental techniques,[6,8−15] i.e., velocity mapping and slice imaging (ion imaging), time-of-flight mass spectrometry, and Doppler profile measurements, have been developed to measure the orientation and alignment effects that often manifest themselves as a relatively small fraction of the total signal. Photofragment alignment and/or orientation of halogen atoms resulting from the photodissociation of a variety of diatomic molecules has been successfully measured: Cl($^2P_{3/2}$) atoms from the photodissociation of Cl_2,[6,9,10,16−18] ICl,[6] and BrCl;[19] and Br($^2P_{3/2}$) from

† Part of the special issue "Richard Bersohn Memorial Issue".

* To whom correspondence should be addressed. E-mail. alex.brown@ualberta.ca.

‡ E-mail: gabriel.balint-kurti@bristol.ac.uk.

10.1021/jp0497615 CCC: $27.50 © 2004 American Chemical Society
Published on Web 05/01/2004

the dissociation of Br_2.[9] More recently, Rakitzis et al.[20] have measured Cl and Br alignment from the photodissociation of HCl and HBr, respectively. However, despite all the detailed experimental measurements, and, although there have been tremendous advances in the phenomenological theory, the applications of the theory to the ab initio determination of the $\mathbf{a}_Q^{(K)}$(p) parameters for specific molecular photodissociation processes has been sparse.[21−24]

As with many dynamics studies, one of the main theoretical hurdles to overcome is the accurate calculation of the electronic structure that underpins the dynamics. Also, for many (all) of the systems studied experimentally, nonadiabatic coupling processes define much of the dynamics, and theoretical methods for dealing with them correctly are therefore crucial. However, unlike many of the other molecules considered experimentally, e.g., the halogens and the interhalogens, for which these theoretical pitfalls exist and are extremely difficult to overcome (though not intractable), quantitative ab initio static and dynamic calculations are feasible for HCl; as proven by the computation of several other properties (total cross-sections, excited state chlorine branching fraction) that agree quantitatively with experiment.[25,26]

Since hydrogen chloride represents one of the simplest systems that dissociates to yield open shell fragments, its photochemistry has been the subject of many previous experimental and theoretical studies.[25−39] In particular, the photodissociation process

$$\begin{aligned} \mathrm{HCl} + h\nu &\rightarrow \mathrm{H}(^2\mathrm{S}) + \mathrm{Cl}(^2\mathrm{P}_{3/2}) \\ &\rightarrow \mathrm{H}(^2\mathrm{S}) + \mathrm{Cl}(^2\mathrm{P}_{1/2}) \end{aligned} \quad (1)$$

is of interest. The chlorine spin−orbit states are customarily designated as Cl and Cl* for $Cl(^2P_{3/2})$ and $Cl(^2P_{1/2})$, respectively. However, in all of these experimental and theoretical studies, except for the recent work[20,23] of Rakitzis et al., the major focus has been on the determination of scalar properties (see also the theoretical work[21] of Balint-Kurti et al. on the photodissociation of the analogous HF molecule)[21] i.e., the total cross-section and the branching fraction measuring the ratio of the yield of spin−orbit excited halogen atoms to total yield, or on the lowest order ($K = 0$) anisotropy parameter β.

In the present work, we report the $\mathbf{a}_Q^{(K)}$(p) parameters ($K \leq 3$) describing the alignment/orientation of Cl fragments produced from the photodissociation of HCl and DCl as determined from a quantum mechanical time-dependent wave packet calculation based on ab initio potential energy curves, spin−orbit couplings, and dipole moments. These ab initio potential energy curves have been used previously[25,26,28] to determine the scalar properties, i.e., total cross-section and branching fractions, for the HCl and DCl photofragmentation processes and to provide a quantitative interpretation of the corresponding experimental measurements.

The paper is organized in the following manner. Section 2 briefly reviews the theory for determining the anisotropy parameters, and, in particular, includes details relevant for the photodissociation of HCl and DCl. Section 2.1 outlines the underlying electronic structure as it relates to the two lowest energy asymptotes $H(^2S_{1/2}) + Cl(^2P_{3/2})$ and $H(^2S_{1/2}) + Cl(^2P_{1/2})$, which are the only ones of interest here. The time-dependent wave packet treatment of the dynamics, is discussed in Section 2.2, with an emphasis on the determination of the photofragmentation **T** matrix elements. Section 2.3 presents the methods used to calculate the dynamical factors, $f_K(q,q')$ and the alignment and polarization coefficients, $\mathbf{a}_Q^{(K)}(p)$, from the photofragmentation **T** matrix elements. The resulting vector correlation coefficients for the photodissociation of HCl and DCl molecules are presented as a function of the photolysis wavelength in Section 3. In this section, proposals for experiments that would verify our predictions are also made and are briefly discussed. Section 4 presents a discussion of various dynamical models that have been widely used to interpret diatomic photodissociation processes and finally a short summary of the work is given in Section 5.

2. Theory

The theoretical ab initio treatment of the photodissociation process requires three important parts: (1) the underlying electronic structure and the computation of the potential energy curves and other molecular parameters; (2) a methodology for performing the dynamics, with the added requirement, that the nonadiabatic processes are correctly accounted for, and (3) a way to extract the orientation and alignment parameters $\mathbf{a}_Q^{(K)}(p)$ from the information acquired during the dynamical calculations. Once the dynamics have been dealt with properly using ab initio data of high quality for the underlying electronic structure, the $\mathbf{a}_Q^{(K)}(p)$ can be computed from the photofragmentation **T** matrix elements utilizing a well-established theoretical framework.[4,5,8,10] Photofragmentation **T** matrix elements can be determined from a quantum mechanical, time-dependent wave packet treatment of the photodissociation process.[21,40−42] Calculation of the photofragmentation **T** matrix elements utilizes the transition dipole moment curves, information about the state symmetries and the nonadiabatic couplings. The resulting **T** matrix contains all possible information about the outcome of the dissociation process and about all coherences between different product states. Because much of the theory has been presented elsewhere, we discuss each of these elements only briefly insofar as they apply to the photodissociation of HCl.

2.1 Electronic Structure. If spin−orbit coupling is not taken into account, Λ, S^2, and Σ are good quantum numbers and four electronic states, i.e., $X^1\Sigma^+$ (nondegenerate), $a^3\Pi$ (6-fold degenerate), $A^1\Pi$ (doubly degenerate), and $t^3\Sigma$ (3-fold degenerate), correlate with the lowest energy asymptote $H(^2S) + Cl(^2P)$. This makes a total of 12 electronic states which we refer to as diabatic basis and which together constitute a diabatic basis. The spin−orbit interaction acts as a coupling between these diabatic states. There have been numerous theoretical investigations of these electronic states,[25,26,35,38,39,43−46] including several explicitly examining the spin−orbit coupling between them. We choose to utilize the potential energy curves (PECs), the associated transition dipole matrix ($A^1\Pi \leftarrow X^1\Sigma^+$), the permanent dipole moments ($X^1\Sigma^+$ and $a^3\Pi$ states), and the spin−orbit coupling curves that have been computed by Alexander et al.[25] The fully adiabatic PECs can be determined from the diabatic curves and the spin−orbit couplings. In the fully adiabatic basis, obtained by diagonalizing the diabatic energies plus off-diagonal spin−orbit couplings, the spin−orbit interaction is diagonal and the coupling between the states is due to off-diagonal terms in the kinetic energy. At large internuclear distances, the adiabatic states correlate with the $H(^2S_{1/2}) + Cl(^2P_{3/2})$ and $H(^2S_{1/2}) + Cl(^2P_{1/2})$ pairs of fragments. The analysis of the outcome of the dynamics must be performed in terms of the adiabatic states. The channel correlating with Cl* lies 881 cm^{-1} above that for Cl.[47] The 12 diabatic states transform into 12 adiabatic states upon diagonalization of the matrix containing (diagonal) diabatic energies and the (off-diagonal) spin−orbit coupling matrix elements. The adiabatic states are as follows:

TABLE 1: Theoretical and Experimental[20,23] Alignment and Orientation Parameters for Cl($^2P_{3/2}$) Fragments Produced from HCl Dissociation at 193 nm[a]

	HCl		DCl	
parameter	theory	experiment	theory	range
$\mathbf{a}_0^{(1)}(\perp)$	+0.413	$+0.4 \pm 0.1$	+0.516	±0.775
$\mathbf{a}_0^{(2)}(\perp)$	−0.320	-0.5 ± 0.2	−0.002	±0.800
$\mathbf{a}_2^{(2)}(\perp)$	−0.511	-0.45 ± 0.2	−0.458	±0.566
$Re[\mathbf{a}_1^{(1)}(\parallel, \perp)]$	−0.044	-0.13 ± 0.16	−0.041	±1.162
β	−0.998	-0.97 ± 0.03	−0.998	−1.0...2.0

[a] The experimental error bars are 2σ. Also given is the allowed range for each parameter.

TABLE 2: Theoretical and Experimental[20,23] Alignment and Orientation Parameters for Cl($^2P_{1/2}$) Fragments Produced from HCl Dissociation at 193 nm[a]

	HCl		DCl	
parameter	theory	experiment	theory	range
$\mathbf{a}_0^{(1)}(\perp)$	+0.577	$+0.6 \pm 0.14$	+0.577	±0.577
$Re[\mathbf{a}_1^{(1)}(\parallel, \perp)]$	+0.1006	0.3 ± 0.2	+0.038	±0.866
β	−0.989	-0.87 ± 0.03	−0.964	−1.0...2.0

[a] The experimental error bars are 2σ. Also given is the allowed range for each parameter.

$X^1\Sigma_{0+}$ (ground state); $A^1\Pi_1$ (two substates); $a^3\Pi_1$ (two substates); $t^3\Sigma_1$ (two substates); the $a^3\Pi_2$ (two substates); $a^3\Pi_{0+}$; $a^3\Pi_{0-}$; and $t^3\Sigma_{0-}$. The term symbols translate as a mixed Hund's case(a)/case (c) according to $^{2S+1}L_\Omega$. For Hund's case (c), Ω is the only good quantum number and the ^{2S+1}L labels designate the largest case(a) contribution within the Franck−Condon region, see Figure 6 of ref 28 and the discussion therein for a more complete explanation. The case (a) and case (c) labels correspond to the diabatic and adiabatic representations, respectively. Figure 1 illustrates the ground electronic state ($X^1\Sigma_{0+}$) plus the optically accessible ($\Delta\Omega = 0, \pm 1$) excited electronic states; $\Omega = 2$ and $\Omega = 0^-$ states have been omitted for clarity.

As in our previous studies of hydrogen halides,[21,28,41,48] the effect of rotation on the dynamics has been neglected. An early study[38] showed that for HCl, the overall rotation has very little effect on the photodissociation dynamics as the dissociation takes place in a much shorter time than the rotational period. Previous theoretical studies of HCl dissociation[25,38,49] have examined the role of rotational couplings on the photodissociation dynamics and have predicted no significant effect; as expected, since the dissociation time for HCl is much less than the rotational time. Also, the data in Table 2 of ref 28 provides direct experimental evidence that parent molecule rotation has a negligible influence on the UV photodissociation dynamics. Since rotational coupling is neglected, the only adiabatic states involved in the photodissociation dynamics are the two $\Omega' = 0^+$ states ($X^1\Sigma_{0+}$ and $a^3\Pi_{0+}$) and the six $\Omega' = 1$ states (two each of $A^1\Pi_1$, $a^3\Pi_1$, and $t^3\Sigma_1$). The initial excitation involves perpendicular ($\Delta\Omega = \pm 1$) transitions from the $X^1\Sigma_{0+}$ state to the $A^1\Pi_1$, $a^3\Pi_1$, and $t^3\Sigma_1$ states. These transitions arise from the diabatic spin-allowed $A^1\Pi \leftarrow X^1\Sigma^+$ transition where the nominally spin-forbidden $a^3\Pi_1 \leftarrow X^1\Sigma_{0+}$ and $t^3\Sigma_1 \leftarrow X^1\Sigma_{0+}$ transitions gain transition strength due to the spin−orbit mixing of the $A^1\Pi$, $a^3\Pi$, and $t^3\Sigma$ diabatic states. Unlike in the analogous HF case,[21,41,48] the initial excitation also involves a minor parallel component,[20,26,32] $a^3\Pi_{0+} \leftarrow X^1\Sigma_{0+}$, that arises due to the spin−orbit mixing of the $X^1\Sigma^+$ and $a^3\Pi$ diabatic states.

For the ground-state Cl($^2P_{3/2}$) fragment, the above treatment implies that there are five states contributing to the angular distributions (orientation/alignment) of this fragment. The $a^3\Pi_1$ and $A^1\Pi_1$ states accessed through perpendicular excitation ($\Delta\Omega = \pm 1$) correlate adiabatically as

$$\mathrm{HCl}(a^3\Pi_1;\Omega' = \pm 1) \rightarrow \mathrm{H}(m_\mathrm{H} = \pm 1/2) + \mathrm{Cl}(m_\mathrm{Cl} = \pm 1/2) \quad (2)$$

and

$$\mathrm{HCl}(A^1\Pi_1;\Omega' = \pm 1) \rightarrow \mathrm{H}(m_\mathrm{H} = \mp 1/2) + \mathrm{Cl}(m_\mathrm{Cl} = \pm 3/2) \quad (3)$$

The $X^1\Sigma_{0+}$ state, which only gains population via nonadiabatic recoupling from the $a^3\Pi_{0+}$ state, correlates equally with both $\pm 1/2$ m_H and $\mp 1/2$ m_Cl states, i.e.

$$\mathrm{HCl}(X^1\Sigma_{0+};\Omega' = 0^+) \rightarrow \mathrm{H}(m_\mathrm{H} = \pm 1/2) + \mathrm{Cl}(m_\mathrm{Cl} = \mp 1/2) \quad (4)$$

On the other hand, only three excited states contribute to the angular distribution of the excited-state Cl($^2P_{1/2}$) fragment. The $t^3\Sigma_1$ state correlates as

$$\mathrm{HCl}(t^3\Sigma_1;\Omega' = \pm 1) \rightarrow \mathrm{H}(m_\mathrm{H} = \pm 1/2) + \mathrm{Cl}^*(m_\mathrm{Cl} = \pm 1/2) \quad (5)$$

and the $a^3\Pi_{0^+}$ state, which correlates equally with both $\pm 1/2$ m_H and $\mp 1/2$ m_{Cl}* states, as

$$\mathrm{HCl}(^3\Pi_{0+};\Omega' = 0) \rightarrow \mathrm{H}(m_\mathrm{H} = \pm 1/2) + \mathrm{Cl}^*(m_\mathrm{Cl} = \mp 1/2) \quad (6)$$

The molecular wave functions corresponding to these asymptotes are given in Table 2 of ref 21.

Employing both the adiabatic and diabatic basis sets and the transformation between them, we can proceed to utilize a quantum mechanical time-dependent wave packet treatment to study the dissociation dynamics. As we shall see later, the long-range correlations given in eqs 2−6 are required for a determination of the orientation and alignment parameters $\mathbf{a}_Q^{(K)}(p)$.

2.2 Dynamics. Using a time-dependent wave packet formalism,[40,42,50−53] the initial step in the calculation of the photofragmentation **T** matrix elements is the setting up of an initial wave packet, or, as is the case here, wave packets. The initial (adiabatic) wave packet for electronic state n may be written as

$$\phi_n(R, t = 0) = \mathbf{d}_{q'}^n(R)\Psi_{\Omega_i}(R) \quad (7)$$

where $\phi_n(R, t = 0)$ represents an initial wave packet on the n^{th} electronically adiabatic potential energy surface, $\mathbf{d}_{q'}^n(R)$ is the (adiabatic) transition dipole moment for excitation from the initial electronic state to the excited electronic state n, and $\Psi_{\Omega_i}(R)$ is the ground electronic state nuclear wave function. q' is the vector spherical harmonic component of the transition dipole moment function. It is determined by the symmetries of the initial and upper electronic states. For all calculations reported here, the nuclear wave function corresponds to the $v = 0$ vibrational state, and has been computed using the Fourier grid Hamiltonian method.[50,54,55]

Once the initial wave packets are created (initial excitation takes place), they are propagated forward in time by solving the time-dependent Schrodinger equation with special care taken to properly account for the nonadiabatic dynamics.[28,41] This requires the simultaneous solution of coupled time-dependent

equations (for a more complete discussion, see ref 41) using the excited electronic state PECs and the couplings between them. Unlike in our previous theoretical study of the vibrationally mediated photodissociation of HCl,[28] the coupling of the two $\Omega = 0^+$ states ($X^1\Sigma_{0^+}$ and $a^3\Pi_{0^+}$) is included in order to obtain the $\mathrm{Re}[\mathbf{a}_1^{(1)}(\|, \perp)]$ parameter correctly, see Section 3, for both the $Cl(^2P_{3/2})$ and $Cl(^2P_{1/2})$ fragments. The $X^1\Sigma_{0+}$ state which correlates with the $Cl(^2P_{3/2})$ fragment, see eq 4, only receives population due to recoupling of initial excitation to $a^3\Pi_{0+}$ back to this state due to nonadiabatic processes as the dynamics proceeds. If the $a^3\Pi_{0+} \rightarrow X^1\Sigma_{0+}$ nonadiabatic coupling were ignored, the parallel contribution to the $Cl(^2P_{3/2})$ fragment dissociation cross-section would be identically zero, and it is known[20,26,32] that this contribution is not zero. As in our previous studies of hydrogen halide dissociation,[21,28,41,48] we assume the axial recoil approximation is valid, i.e., the body-fixed projection of the total angular momentum on the molecular axis (Ω) is treated as a good quantum number. This is equivalent to neglect of the overall rotation of the molecule.

The energy dependent photofragmentation **T** matrix element associated with channel n has been shown previously[21,40] to be given by

$$\langle \Psi^-_{n,\Omega}(R, E)|\hat{\mathbf{d}}_q|\Psi_{\Omega_i}\rangle = i\left(\frac{h^2 k_v}{2\pi\mu}\right)^{1/2} \exp(-ik_v R_\infty) A_n(R_\infty, E) \tag{8}$$

where k_v is the asymptotic wave vector for this channel and μ is the reduced mass of the two photofragments. The energy dependent coefficients $A_n(R_\infty, E)$ are obtained by taking the Fourier transform over time of cuts through the time-dependent wave packets, $\phi_n(R_\infty, t)$, at a fixed large value of the scattering coordinate, R_∞, (such that there is no longer coupling between the adiabatic states)[28,40,41]

$$A_n(R_\infty, E) = \frac{1}{2\pi}\int_0^\infty \phi_n(R_\infty, t)\exp[i(E_i + h\nu)t/\hbar]dt \tag{9}$$

2.3 Determination of Dynamical Functions and $a_Q^{(K)}(p)$ Parameters. A discussion of the determination of the dynamical functions for a diatomic molecule AB dissociating into atoms A and B having angular momenta j_A and j_B, respectively, is first presented. The details for HCl follow the general discussion.

Once the photofragmentation **T** matrix elements,[56,57] $\langle \Psi^-_{n,\Omega}(R, E)|\hat{\mathbf{d}}_q|\Psi_{\Omega_i}\rangle$, have been determined using the time-dependent wave packet formalism,[40,50−53] the dynamical functions,[4,10] which are defined as

$$f_K(q,q') = \sum_{n,\Omega,\Omega_A,n',\Omega',\Omega'_A} (-1)^{K+j_A+\Omega'_A} \begin{pmatrix} j_A & j_A & K \\ -\Omega_A & \Omega'_A & q-q' \end{pmatrix} \times T^{n\Omega}_{j_A\Omega_A j_B\Omega_B} (T^{n'\Omega'}_{j_A\Omega_A j_B\Omega_B})^* \times \langle \Psi^-_{n,\Omega}(R, E)|\hat{\mathbf{d}}_q|\Psi_{\Omega_i}\rangle^* \langle \Psi^-_{n',\Omega'}(R, E)|\hat{\mathbf{d}}_{q'}|\Psi_{\Omega_i}\rangle \tag{10}$$

can be calculated. The indices q,q' are the vector spherical harmonic components[58,59] of the molecular electric dipole moment with respect to the recoil axis. They can take only the values 0 or ± 1, corresponding to parallel or perpendicular electronic transitions, respectively. $\Psi^-_{n,\Omega}(R, E)$ is the scattering wave function for the channel n, Ω in the body-fixed coordinate system. The initial and final z-components of the total electronic angular momentum about the molecular axis are related by $\Omega = \Omega_i + q$.

There is no explicit summation over Ω_B in eq 10 as the conservation relationship $\Omega = \Omega_A + \Omega_B$ ensures that this summation is effectively performed. In the definition of the dynamical factors, eq 10, only Ω_B and j_B occur and not Ω'_B or j'_B since the average or trace over these quantum numbers has been taken. The relationship $q - q' = \Omega_A - \Omega'_A = \Omega - \Omega'$ is fulfilled due to the symmetry properties of $3j$ symbols. Therefore, the diagonal elements of the dynamical functions $f_K(q, q')$ with $q = q'$ correspond to incoherent excitation of parallel, or perpendicular transitions, while the off-diagonal elements with $q \neq q'$ correspond to coherent excitation of different molecular continua. The off-diagonal terms are responsible for interference effects in the vector properties.

The expression for the dynamical functions of fragment B can be obtained from eq 10 by exchanging subscripts A and B. In general, the dynamical functions relevant for a particular photofragment with angular momentum j_A a range from $K = 0$ to $K = 2j_A$,[4,60] where K is referred to as the multipole rank. The terminology "multipole rank" is used as the dynamical functions are directly related to the angular momentum state multipoles, $\rho^{j_A}_{KQ}(\theta,\phi)$, see eq 5 of ref 21 and the discussion in ref 4. The description of the hydrogen atom fragment ($j_A = 1/2$) from the photolysis therefore requires only state multipoles (dynamical functions) of rank $K = 0$ (population) and $K = 1$ (orientation, dipole moment). For the ground-state chlorine fragment ($j_B = 3/2$), the complete set of state multipoles (dynamical functions) contains $K = 0$, $K = 1$, and also $K = 2$ (alignment, quadrupole moment) and $K = 3$ (orientation, octupole moment) while for the excited-state chlorine fragment ($j_B = 1/2$) only $K = 0$ and $K = 1$ dynamical functions are required.

The symmetry relationships[61]

$$f_K(q,q') = (-1)^K f_K(-q,-q') = (-1)^{q-q'} f^*_K(q', q) \tag{11}$$

are obeyed by the dynamical functions. These dynamical functions, $f_K(q,q')$, are constructed from the photofragmentation **T** matrix elements and contain all information about the photodissociation dynamics. While the $f_K(q,q')$ contain all this molecular information, the quantum mechanical observables that can be determined experimentally are the magnitude of the total cross section, σ_0, and the dimensionless anisotropy parameters, which are normalized combinations of the dynamical functions of rank K. The zeroth-rank anisotropy parameter is the well-known β parameter.[58,62] In terms of the $K = 0$ dynamical functions, β is given as[4]

$$\beta = \frac{2[f_0(0,0) - f_0(1,1)]}{2f_0(1,1) + f_0(0,0)} \tag{12}$$

For rank $K > 0$, two alternative sets of anisotropy parameters have been introduced recently: one set[5,18,63] $\mathbf{a}_Q^{(K)}(p)$ relates to the molecular frame and the other set,[7,8] α_K, γ_K, η_K, and s_K, to the laboratory frame orientation and alignment of the photofragment angular momenta. The $\mathbf{a}_Q^{(K)}(p)$ set of orientation and alignment parameters, where $p = \perp$, $\|$, or $(\|, \perp)$ corresponding to pure perpendicular, pure parallel, or mixed parallel/perpendicular excitation, is most suitable for a theoretical analysis and is therefore used here. The relationship between the two sets for the $\mathbf{a}_Q^{(K)}(p)$, $p = \perp$, parameters has recently been presented.[21]

As discussed above, parameters up to rank $K = 3$ are utilized for describing the chlorine fragments resulting from HCl photodissociation. The parameters discussed in Section 3 include

three parameters describing incoherent perpendicular excitation [$\mathbf{a}_0^{(1)}(\perp)$, $\mathbf{a}_0^{(2)}(\perp)$, and $\mathbf{a}_0^{(3)}(\perp)$], two parameters describing coherent perpendicular excitation [$\mathbf{a}_2^{(2)}(\perp)$ and $\mathbf{a}_2^{(3)}(\perp)$], and a single parameter describing coherent parallel and perpendicular excitation [$\mathbf{a}_1^{(1)}(\parallel, \perp)$]. As only a single state accessed by parallel excitation correlates with each asymptote, no parallel (only) parameters are computed. The parameters describing incoherent perpendicular excitation are related to the dynamical functions by

$$\mathbf{a}_0^{(1)}(\perp) = \frac{f_1(1,1)}{f_0(1,1)} \tag{13}$$

$$\mathbf{a}_0^{(2)}(\perp) = V_2(j_{Cl})^{-1}\frac{f_2(1,1)}{f_0(1,1)} \tag{14}$$

and

$$\mathbf{a}_0^{(3)}(\perp) = V_3(j_{Cl})^{-1}\frac{f_3(1,1)}{f_0(1,1)} \tag{15}$$

Those for coherent perpendicular excitation are

$$\mathbf{a}_2^{(2)}(\perp) = -\frac{1}{2}V_2(j_{Cl})^{-1}\frac{f_2(1,-1)}{f_0(1,1)} \tag{16}$$

and

$$\mathbf{a}_2^{(3)}(\perp) = \frac{i}{2}V_3(j_{Cl})^{-1}\frac{f_3(1,-1)}{f_0(1,1)} \tag{17}$$

The factors $V_2(j_{Cl})$ and $V_3(j_{Cl})$ are given by

$$V_2(j) = \left[\frac{j(j+1)}{(2j+3)(2j-1)}\right]^{1/2} \tag{18}$$

and

$$V_3(j) = \frac{j(j+1)}{[(j-1)(j+2)(2j-1)(2j+3)]^{1/2}} \tag{19}$$

The parameter Re $[\mathbf{a}_1^{(1)}(\parallel, \perp)]$ describing coherent parallel and perpendicular excitation is

$$\mathrm{Re}[\mathbf{a}_1^{(1)}(\parallel, \perp)] = \frac{-3\sqrt{2}\mathrm{Re}[f_1(1,0)]}{2f_0(1,1) + f_0(0,0)} \tag{20}$$

Note that there are other parameters describing coherent parallel and perpendicular excitation, e.g., Im $[\mathbf{a}_1^{(1)}(\parallel, \perp)]$, but we choose to present results only for Re $[\mathbf{a}_1^{(1)}(\parallel, \perp)]$ which has been experimentally determined for HCl.[20]

The anisotropy parameters $\mathbf{a}_Q^{(K)}(p)$ have clear physical meaning. In general, the molecular frame state multipoles associated with orientation and alignment of the photofragment angular momentum distributions are functions of the parameter β, see eq 12, and of the angle θ describing the direction of the recoil axis Z relative to the space-fixed z axis.[8,10] The space-fixed z axis is taken to be the direction of the light polarization vector $\hat{\mathbf{e}}$ for linearly polarized photodissociation light and the propagation direction of the light in the case of circularly polarized photodissociation light. For circularly polarized light, the angle θ_c describing the recoil axis relative to the light propagation direction should be used instead of the angle θ.

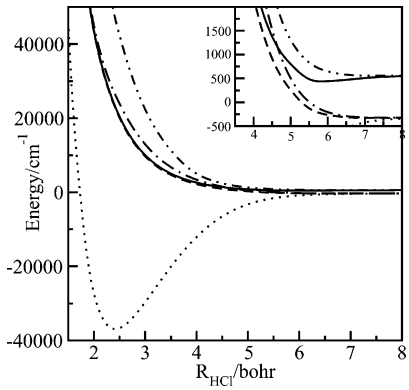

Figure 1. The fully adiabatic potential energy curves as a function of the HCl bond length as determined using the data from ref 25. All potential energies are for $J = 0$. The inset illustrates an expanded view of the asymptotic region of the potentials. The potentials, in order of increasing energy in the asymptotic region are $X^1\Sigma_{0+}$ (dotted line), $a^3\Pi_1$ (dash−dot line), $A^1\Pi_1$ (dashed line), $a^3\Pi_{0+}$ (solid line), and $t^3\Sigma_1$ (dot−dot−dash line).

The anisotropy parameters $\mathbf{a}_Q^{(K)}(p)$ are equal to the values of the corresponding familiar body frame fragment alignment parameters,[58] i.e., A_{KQ}, for selected values of β and θ (see Appendix A).

The anisotropy parameters $\mathbf{a}_0^{(2)}(\perp)$, $\mathbf{a}_2^{(2)}(\perp)$, and $\mathbf{a}_2^{(3)}(\perp)$ in eqs 14, 16, and 17, respectively, can be measured using linearly or circularly polarized light. On the other hand, some of the parameters, i.e., $\mathbf{a}_0^{(K)}(\perp)$, $K = 1$, 3 in eqs 13 and 15, respectively, and Re$[\mathbf{a}_1^{(1)}(\parallel, \perp)]$ in eq 20, can only be measured using circularly polarized photodissociation light. Hence, it is suitable to associate some of the anisotropy parameters with linearly polarized light, i.e., those that can be detected with either polarization, and some of them with circularly polarized light, i.e., those that can be detected only with circularly polarized light.

The photofragment nuclear spins have been neglected in the above description. Since the duration of the dissociation process (less than 100 fs) is much smaller than the Heisenberg uncertainty time, $\Delta t = \hbar/(2\Delta E)$, associated with the hyperfine splitting in the atoms (on the order of ns for H and Cl), this assumption is justified. While the nuclear spins do not affect the photodissociation dynamics, the hyperfine interaction in the final fragments is important as it results in partial depolarization of the fragment's electron angular momenta.[58]

3. Results and Discussion

All results discussed for Cl($^2P_{3/2}$) and Cl($^2P_{1/2}$) are for the ^{35}Cl isotope. Calculations performed for ^{37}Cl are graphically indistinguishable from those for ^{35}Cl, i.e., are within much less than 1% of the ^{35}Cl values, and, thus, would be experimentally indistinguishable. The similarity of the results upon chlorine isotopic substitution is due to the extremely small (<0.3%) changes in the reduced masses of the systems.

3.1 Anisotropy Parameters for Cl($^2P_{3/2}$). Recall that the angular distribution for Cl($^2P_{3/2}$) is described by anisotropy parameters up to rank $K = 3$, whereas that for Cl($^2P_{1/2}$) requires parameters only up to rank $K = 1$. Figure 2 illustrates the anisotropy parameters describing incoherent perpendicular excitation, $\mathbf{a}_0^{(K)}(\perp)$, for the ground-state Cl($^2P_{3/2}$) fragment produced from the photodissociation of HCl and isotopically substituted DCl as a function of photolysis wavelength. The results are for excitation from the ground $v = 0$ vibrational state. Also shown are the experimental measurements of $\mathbf{a}_0^{(1)}(\perp)$ and

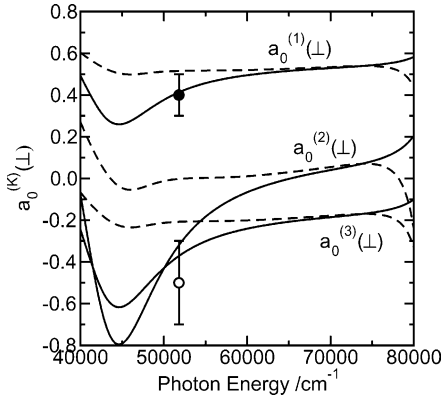

Figure 2. Incoherent anisotropy parameters $\mathbf{a}_0^{(K)}(\perp)$ for the production of ground-state Cl($^2P_{3/2}$) as a function of photon energy for the photodissociation of HCl (solid lines) and DCl (dashed lines) initially in their ground, $v = 0$, vibrational states. Also shown are the experimental measurements for $\mathbf{a}_0^{(1)}(\perp)$ (●) and $\mathbf{a}_0^{(2)}(\perp)$ (○) of Rakitzis et al.[20,23] for HCl photodissociation at 193 nm.

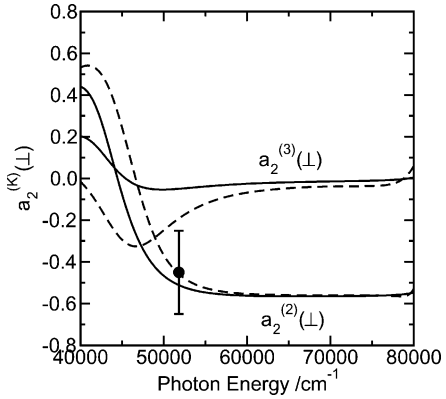

Figure 3. Coherent anisotropy parameters $\mathbf{a}_2^{(K)}(\perp)$ for the production of ground-state Cl($^2P_{3/2}$) as a function of photon energy for the photodissociation of HCl (solid lines) and DCl (dashed lines) initially in their ground, $v = 0$, vibrational states. Also shown is the experimental measurement for $\mathbf{a}_2^{(K)}(\perp)$ (●) of Rakitzis et al.[20] for HCl dissociation at 193 nm.

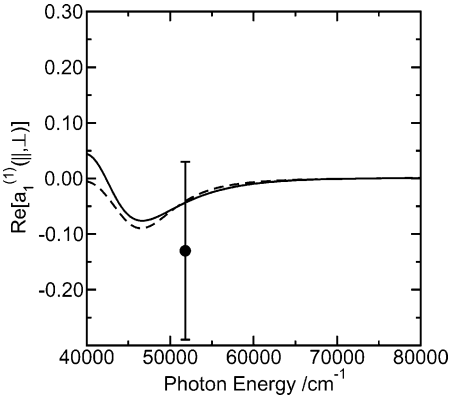

Figure 4. Coherent anisotropy parameters Re[$\mathbf{a}_1^{(1)}$(||, $\perp$) for the production of ground-state Cl($^2P_{3/2}$) as a function of photon energy for the photodissociation of HCl (solid lines) and DCl (dashed lines) initially in their ground, $v = 0$, vibrational states. Also shown is the experimental measurement of Rakitzis et al.[23] for HCl dissociation at 193 nm.

$\mathbf{a}_0^{(2)}(\perp)$ for Cl($^2P_{3/2}$) following HCl photolysis at 193 nm made by Rakitzis et al.[20] The theoretical results for Cl($^2P_{3/2}$) produced from photodissociating HCl and DCl at 193 nm along with the experimentally measured parameters[20,23] are presented in Table 1. The agreement between the theoretical and experimental results for $\mathbf{a}_0^{(1)}(\perp)$ for HCl is excellent, see Table 1. Although the agreement between theory and experiment for $\mathbf{a}_0^{(2)}(\perp)$ is not quite as good, in the vicinity of the experimental measurement at 193 nm, there is a very strong dependence on photolysis wavelength of the $\mathbf{a}_0^{(2)}(\perp)$ parameter (see Figure 2). Because the $\mathbf{a}_0^{(3)}(\perp)$ parameter provides only a small correction to the fit to the experimentally measured signal, it has not yet been determined with sufficient accuracy to warrant a comparison with the theoretical results.[64] Also, the $\mathbf{a}_0^{(3)}(\perp)$ parameter does not provide any new information that is not carried by the $\mathbf{a}_0^{(1)}(\perp)$ and $\mathbf{a}_0^{(2)}(\perp)$ parameters, and, thus, while its calculation is performed here for completeness, its determination, whether theoretical or experimental, does not provide any new insight into the dynamics.

Although Figure 2 shows that there are significant similarities in the behavior of the $\mathbf{a}_0^{(K)}(\perp)$ parameters as a function of photolysis frequency for the Cl produced from HCl and DCl, there are also significant differences *between* the isotopomers (see Table 1). In particular, the Cl($^2P_{3/2}$) produced from HCl is strongly aligned [cf., $\mathbf{a}_0^{(2)}(\perp)$], whereas that produced from DCl exhibits essentially no alignment, i.e., $\mathbf{a}_0^{(2)}(\perp) \approx 0$. Therefore, it will be interesting to see if the isotope difference for the $\mathbf{a}_0^{(K)}(\perp)$ can be experimentally confirmed as has been done for the (scalar) branching fraction Γ.[26,30]

The $\mathbf{a}_2^{(K)}(\perp)$ parameters describing the coherent perpendicular excitation of the $a^3\Pi_1$ and $A^1\Pi_1$ states are illustrated in Figure 3 for the Cl($^2P_{3/2}$) fragment arising from the photodissociation of HCl and DCl from $v = 0$. The $\mathbf{a}_2^{(2)}(\perp)$ parameter describes the degree of coherence between pairs of m states, m and $m \pm 2$. Also shown is the experimental measurement[23] of $\mathbf{a}_2^{(2)}(\perp)$ for Cl($^2P_{3/2}$) produced from HCl dissociation at 193 nm. The theoretically determined parameters are relatively constant over the energy range 55 000−80 000 cm^{-1}. However, they depend strongly on photolysis energy in the low-energy (long wavelength) region below 55 000 cm^{-1}. This is particularly interesting since the low-energy region is where most experimental measurements of the branching fraction have taken place. As with the $\mathbf{a}_0^{(K)}(\perp)$ parameters, there are fairly significant differences between the $\mathbf{a}_2^{(K)}(\perp)$ parameters for HCl and DCl. The calculated difference awaits experimental verification, but this may be difficult to obtain since the differences are relatively small for the $\mathbf{a}_2^{(2)}(\perp)$ parameters and for the $\mathbf{a}_2^{(3)}(\perp)$ parameters, where the differences between HCl and DCl are much greater, the experimental measurements are much more difficult.

Figure 4 illustrates the Re[$\mathbf{a}_1^{(1)}$(||, $\perp$)] parameter describing the coherent parallel and perpendicular excitation as a function of photolysis wavelength for Cl($^2P_{3/2}$) photofragments from HCl($v = 0$) and DCl($v = 0$) dissociation. The experimental measurement at 193 nm[20] is also presented. This parameter provides direct information about the interference between the parallel ($X^1\Sigma_{0+}$ state populated via nonadiabatic coupling from $a^3\Pi_{0+}$) and perpendicular ($A^1\Pi_1$ and $a^3\Pi_1$) states contributing to the production of Cl($^2P_{3/2}$). Although the theoretical results agree with experiment to within the experimental uncertainty, the discrepancy between the two is larger than for the corresponding $\mathbf{a}_0^{(K)}(\perp)$ results. The larger discrepancy could possibly be attributed as follows. The experimental β parameter measurement for Cl($^2P_{3/2}$) at 193 nm[20] shows that the contribution from the direct parallel excitation $^3\Pi_{0+} \leftarrow {}^1\Sigma_{0+}$ transition is about 1% (±1%). The parallel contribution to Cl($^2P_{3/2}$) production therefore arises almost entirely through nonadiabatic electronic coupling from the excited $^3\Pi_{0+}$ state down to the ground $^1\Sigma_{0+}$

state. While the theoretical value for β (0.9984) is within the experimental error bars (0.97 ± 0.03), it is possible that the parallel contribution is being underestimated; an underestimation that may also lead to the discrepancy between the experimental and theoretical Re[$\mathbf{a}_1^{(1)}$(∥, ⊥)] parameters.

The computed absorption cross-section for HCl(v = 0) peaks at ≈ 65 000 cm^{-1} and has a fwhm of ≈ 12 000 cm^{-1}, i.e., the cross-section has significant values when depicted graphically over the energy range 47 500 to 82 500 cm^{-1}. Therefore, the most significant variations of the $\mathbf{a}_Q^{(K)}(p)$ parameters take place in the low-energy tail of the absorption cross-section. It is interesting to note that this region is that in which the branching fraction, Γ, varies most strongly as seen in experiment and theory for both HCl[26,29] and DCl.[30] Furthermore the experimental measurements of Γ in this region indicate that experimental probing of the photolysis energy-dependence of the $\mathbf{a}_Q^{(K)}(p)$ should be feasible.

3.2 Anisotropy Parameters for Cl(^{2}P$_{1/2}$). The excited-state Cl(^{2}P$_{1/2}$) fragment's angular distribution is fully described by orientation (K = 1) parameters only, unlike the angular distribution of Cl(^{2}P$_{3/2}$) which requires both orientation (K = 1 and K = 3) and alignment (K = 2) parameters.

The $\mathbf{a}_0^{(1)}(\perp)$ parameter describing Cl(^{2}P$_{1/2}$) production is not plotted as it is equal to the maximal value of 0.577 (= $1/\sqrt{3}$), independent of photolysis energy, for both HCl and DCl. The reason that there is no energy dependence of this parameter is that only a single state ($^3\Sigma_{\Omega=+1}$ or $^3\Sigma_{\Omega=-1}$) contributes to the photofragmentation cross-section; the particular state involved depends on whether right- or left-circularly polarized light is utilized in the dissociation.[23] Rakitzis et al.[23] have confirmed this experimentally by measuring a value of 0.6 ± 0.14 at 193 nm. On the other hand, the Re[$\mathbf{a}_1^{(1)}$(∥, ⊥)] parameter describing coherent parallel and perpendicular excitation does show a strong photolysis energy dependence especially at low energy, see Figure 5. Below 60 000 cm^{-1}, there are clear differences between the calculated Re[$\mathbf{a}_1^{(1)}$(∥, ⊥)] parameters for Cl(^{2}P$_{1/2}$) produced from HCl and DCl. However, these differences would be well within the experimental error bars, as given by the point measured at 193 nm. While the absolute magnitudes of these parameters would be extremely difficult to measure experimentally, it is possible that the differences (especially at extremely low-energy < 45 000 cm^{-1}) could be measured.

3.3 H Atom Polarization. Spin orientation of the hydrogen atom is extremely difficult to measure directly by laser ionization[65] due to the small excited-state spin−orbit splitting that must be resolved in such an experiment (see, e.g., ref 66). Although the alignment/orientation of the chlorine atom is much more easily measured than that of the H atom, the polarization of the H atom can be readily computed and it was inferred from the experimental measurements of the angular momentum distributions of the ground and excited-state chlorine atoms.[23]

Assuming photodissociation by circularly polarized light via the perpendicular transition, the number of the photofragments N as function of the recoil angle θ_c can be written as

$$N(\theta_c) = \frac{3}{16\pi}(1 + \cos^2\theta_c) \tag{21}$$

Neglecting the (small) contribution from the parallel transitions, the angular dependence of the H atom (H electron) spin polarization is the difference in the population of the spin-up and spin-down states normalized to their sum, $P_e(\theta_c) = (n_+ - n_-)/(n_+ + n_-)$. $P_e(\theta_c)$ can be presented in the molecular frame as[4,8]

$$P_e(\theta_c) = \frac{j_z(\theta_c)}{j} = 2\sqrt{\frac{j+1}{j}}\frac{\mathbf{a}_0^{(1)}(\perp)\cos\theta_c}{1 + \cos^2\theta_c} \tag{22}$$

where $j_z(\theta_c)$ is the expectation value of the component of the electron atomic spin j = 1/2 onto the recoil direction.

In the absence of the parallel transitions, each fragment's angular momentum **j** is "parallel" to the recoil direction,[8] i.e., the largest m-states are populated. eq 22 describes the electron spin polarization for the time after photodissociation that is much shorter than the hyperfine interaction precession period in the H atom (τ_{hf} = 0.7 ns). For longer times, the electron and proton angular momenta are coupled by the nuclear hyperfine interaction, and, therefore, after the dissociation, the polarization oscillates between the two. In the long-time limit, $t \gg \tau_{hf}$, the right-hand side of eq 22 should be multiplied by the depolarization factor 1/2.

It is seen from eqs 21 and 22 that the photofragments moving parallel and antiparallel to the direction of light propagation have maximal values of their electron spin polarization, $P_e^{max} = \sqrt{3}\mathbf{a}_0^{(1)}(\perp)$, whereas the photofragments moving in the perpendicular plane have no spin polarization at all. The total electron spin polarization obtained by projecting all electron spins onto the direction of light propagation and integrating over all recoil directions is

$$P_e^{tot} = \langle P_e(\theta_c)N(\theta_c)\cos\theta_c\rangle = \frac{1}{2}P_e^{max} \tag{23}$$

Due to axial symmetry of the process, the corresponding total photofragment angular momentum $\mathbf{j}_{tot}$ is parallel to the direction of the light propagation.

Rather than plotting the Re [$\mathbf{a}_1^{(1)}$(∥, ⊥] and $\mathbf{a}_0^{(1)}(\perp)$ parameters for the H atom (recall $K \le 1$ since j = 1/2), we present in Figure 6 the maximum polarization degree P_e^{max} weighted average for H-atom (D-atom) produced with Cl and Cl* co- fragments, see eqs 2−6. Clearly, for excitation energies below 55 000 cm^{-1}, highly polarized hydrogen atoms (SPH) can be produced, i.e., $P_e^{max} > 50\%$. On the other hand, the dissociation of DCl does not produce highly spin polarized D-atoms at any frequency. Our result for H-atom production at 193 nm, P_e^{max} = 64%, is in good agreement with the experimental measurement[23] of 72%. The predicted maximum SPH that can be produced is 95% at a dissociation energy of 45 000 cm^{-1} (222 nm). Experimentally, right- or left-circularly polarized light can be used to select Ω' = + 1, or −1, respectively, parallel to the light propagation direction, to produce SPH. For laser pulses much shorter than 0.7 ns, the polarization plotted in Figure 6 can be selected for either electron, or the proton. For laser pulses longer than 0.7 ns, the polarization of both the electron and the proton will be averaged, i.e., half of the plotted value.

4. Dynamical Models

The dynamics presented here are exact (within the limitations of the electronic structure calculations upon which they are based), but it is useful to consider the results within several models for the dissociation of hydrogen halides. Three models have commonly been used to interpret photodissociation processes (1) the adiabatic model, (2) the diabatic or sudden model,[67,68] and (3) the strong coupling or statistical model. All of these models have in common the fact that their predictions are independent of the excitation energy. Each of these models is described briefly below along with predictions for two dissociation properties: the Cl* branching fraction (Γ) and the H atom polarization. Note that the use of these models for

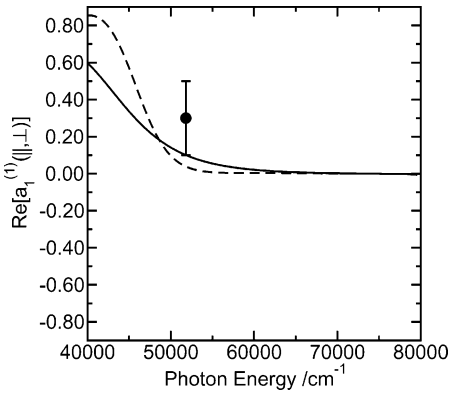

Figure 5. Coherent anisotropy parameters Re[$\mathbf{a}_1^{(1)}$(||, ⊥) for the production of excited-state Cl($^2P_{1/2}$) as a function of photon energy for the photodissociation of HCl (solid lines) and DCl (dashed lines) initially in their ground, $v = 0$, vibrational states. Also shown is the experimental measurement of Rakitzis et al.[23] for HCl dissociation at 193 nm.

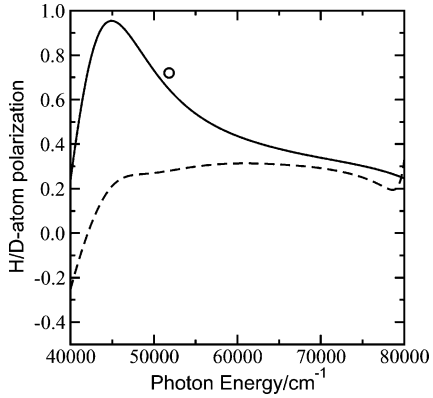

Figure 6. H atom polarization as a function of photon energy for the photodissociation of HCl (solid lines) and DCl (dashed lines) initially in their ground, $v = 0$, vibrational states. Also shown is the experimental measurement of Rakitzis et al.[23] for HCl dissociation at 193 nm.

predicting Γ has been discussed previously,[26,41] and is only included here for completeness. Also, to simplify the discussion, we focus on the $\Omega = \pm 1$ channels neglecting the extremely small $\Omega = 0^+$ components.

In the adiabatic model, it is assumed that the photofragments part so slowly that the system remains on a single electronic state. For HCl, since the primary excitation is to $A^1\Pi_1$, the adiabatic model would predict that the sole dissociation channel would be given by eq 3. Since this would result in a branching fraction of zero ($\Gamma = 0$), this model is clearly incorrect. For circularly polarized light leading to HCl($A^1\Pi_1$, $\Omega' = +1$), the ground-state chlorine will have $m_{Cl} = +3/2$ and the spin orientation of the hydrogen atom electron will consequently be exclusively downward, i.e., $m_H = -1/2$.

In the diabatic, or sudden model, it is assumed that (i) the atoms separate so rapidly that there is no time for the electronic structure to change slowly so as to follow the adiabatic correlation diagram and (ii) the rearranging of all molecular quantum states happens simultaneously in a relatively narrow area of the internuclear distances, i.e., the nonadiabatic transitions mainly occur in the vicinity of a single point $R = R_n$. If these two conditions are fulfilled, the Hund's case (a) molecular wave functions corresponding to the internuclear distances $R < R_n$ can be simply projected onto the product of the free atom wave functions which are eigenfunctions for the distances $R > R_n$

$$|S\Sigma\Lambda\rangle = \sum_{\Omega_A, j_B, \Omega_B} K_{j_A\Omega_A j_B\Omega_B}(S,\Sigma,\Lambda)|j_A\Omega_A\rangle|j_B\Omega_B\rangle \quad (24)$$

where S and Σ are total molecular spin and its projection, Λ is the projection of the total molecular orbital momentum, $j_A = 1/2$, Ω_A and $j_B = 3/2$, 1/2, Ω_B are the total H and Cl angular momenta and their projections, respectively. All of the projections in eq 24 are defined with respect to the internuclear axis.

The expansion coefficients $K_{j_A\Omega_A j_B\Omega_B}(S,\Sigma,\Lambda)$ in eq 24 are as follows:

$$K_{j_A\Omega_A j_B\Omega_B}(S,\Sigma,\Lambda) = \sum_{\mu_2} C^{S\Sigma}_{(1/2)\Omega_A(1/2)\mu_2} C^{j_2\Omega_2}_{(1/2)\mu_2 1\Lambda} \quad (25)$$

where $C^{S\Sigma}_{(1/2)\Omega_A(1/2)\mu_2}$ is a Clebsch-Gordan coefficient.

The hydrogen halides would appear to be excellent candidates for complying with this model, as the speed of the H-atom recoil is enhanced by its light mass relative to the mass of the halogen partner. According to eq 25, the sudden model predicts one-third of the population in the excited Cl* state and two-thirds of the population in the ground electronic state; the resulting branching fraction is 1/3. More interestingly, the ground-state population is produced one-sixth (1/6) in $a^3\Pi_1$ and one-half (1/2) in $A^1\Pi_1$, whereas the spin−orbit excited state is produced one-third (1/3) in $t^3\Sigma_1$. Thus, using eqs 2, 3, and 5, one can conclude that predicted H atom net polarization is zero, which is in contradiction with the result of wave packet calculations shown in Figure 6.

The sudden model fails since necessary condition (ii) as stated above is not fulfilled in the HCl or in the DCl cases. Visual analysis of the wave packet results in ref 28, and reexamined here for $v = 0$, indicates that there are two areas of rearranging of the molecular wave functions in HCl which appear to have little overlap with each other. In the first one, from $R \simeq 3.5$ bohr to $R \simeq 5.5$ bohr, the nonadiabatic transition occurs mainly between the $A^1\Pi_1$ state and the $t^3\Sigma_1$ state, whereas it appears that the $a^3\Pi_1$ state behaves almost adiabatically. In the second area, from $R \simeq 5$ bohr to $R \simeq 8$ bohr, the nonadiabatic transition occurs mainly between the $A^1\Pi_1$ and the $a^3\Pi_1$ states, while the nonadiabatic transitions between each of them and the $t^3\Sigma_1$ state are less pronounced. While the nonfulfillment of condition (ii) leads to the failure of the diabatic model, the (simplistic) view of two distinct regions of nonadiabatic coupling, each involving coupling between only two states, suggests the development of a model based on two inter-related two-state models; preliminary development and results of the model are presented in Appendix B.

In the strong coupling or statistical model, the states are so strongly coupled by the interaction that all accessible states are equally populated. Of course, the result would be a population distribution of 1/3:1/3:1/3 and as such both the branching fraction Γ and the H atom polarization would be 1/3.

Comparing the models' predictions with the results of Figure 6, we see that none of them provides a quantitative (or even qualitative) prediction across the entire energy range. In the low energy region, the HCl results are close to the adiabatic predictions. The HCl results begin to approach the statistical limit (not the diabatic or sudden limit, as might be expected) for high energies. On the other hand, DCl is very nearly at the statistical value across the entire energy range. So in conclusion, all the models must be used with extreme care, if they can be used at all, since they yield only qualitative results (and these only appear to apply in the low and high excitation energy limits). Although some insight can be gathered from them, one

must resort to exact dynamical studies to obtain a "true" picture of the dynamics especially as a function of excitation energy. Therefore, it is clear that great care must be taken when utilizing simple static models to try and predict (or interpret) physical obervables. The best option is to utilize a dynamical treatment, if available, as a guide.

5. Conclusions

The paper presents the first ab initio calculation of the (near) complete set of anisotropy parameters $\mathbf{a}_Q^{(K)}(p)$ describing the $Cl(^2P_{3/2})$ and $Cl(^2P_{1/2})$ angular momentum distributions arising from the photodissociation of HCl and DCl as a function of photon energy. Although results have only been presented for excitation from $v = 0$, calculations have also been performed for photodissociation of vibrationally excited HCl and DCl in their $v = 1$ states.[69] As has been determined for other properties, e.g., branching fractions and total cross-sections, for the vibrationally mediated photodissociation of the hydrogen halides,[28,37,38,70−72] sharp changes in the properties are observed over narrow photon energy ranges due to nodes in the initial vibrational state. Similar behavior is seen[69] for the $\mathbf{a}_Q^{(K)}(p)$ parameters for HCl and DCl—see the analogous result for HF and DF given in ref 21.

The anisotropy parameters as a function of photolysis wavelength for HCl and DCl have been compared, and the theoretical predictions for HCl have been compared to experimentally determined parameters.[20,23] Although the anisotropy parameters for the photodissociation of DCl are similar to those arising from the dissociation of HCl across much of the energy range spanning the total cross-section, they are distinctly different in the low-energy (long wavelength) region. It is interesting to note that the region where the parameters are different is that for which many experimental measurements of the branching fraction have been made.[26,29,30] Therefore, verification of the theoretically predicted difference should be amenable to current experimental techniques.

Appendix A: Relationship of $\mathbf{a}_Q^{(K)}(p)$ to A_{KQ}

The anisotropy parameters $\mathbf{a}_Q^{(K)}(p)$ are equal to the values of the corresponding familiar body frame fragment alignment parameters,[58] A_{KQ}, for selected values of the β and θ (or θ_c). β is the zeroth rank anisotropy parameter, see eq 12. The space-fixed z axis is taken to be the direction of the light polarization vector $\hat{\mathbf{e}}$ for linearly polarized photodissociation light and the propagation direction of the light in the case of circularly polarized light. θ is the angle describing the direction of the photofragment recoil axis Z relative to the space-fixed z axis for linearly polarized light[8,10] while, for circularly polarized light, θ_c is the angle describing the recoil axis relative to the light propagation direction. In particular, the relationships between these two sets of parameters for purely perpendicular transitions are given by

$$\mathbf{a}_0^{(1)}(\perp) = A_{10}^{\mathrm{mol}}(\beta = -1;\ \theta_c = 0) \tag{26}$$

$$\mathbf{a}_0^{(3)}(\perp) = 2A_{30}^{\mathrm{mol}}(\beta = -1;\ \theta_c = 0) \tag{27}$$

$$\mathbf{a}_0^{(2)}(\perp) = A_{20}^{\mathrm{mol}}(\beta = -1) \tag{28}$$

$$\mathbf{a}_2^{(2)}(\perp) = A_{22}^{\mathrm{mol}}(\beta = -1) \tag{29}$$

and

$$\mathbf{a}_2^{(3)}(\perp) = 2A_{32}^{\mathrm{mol}}(\beta = -1) \tag{30}$$

In eqs 26 and 27, the anisotropy parameters $\mathbf{a}_0^{(K)}(\perp)$, $K = 1, 3$, are associated with circularly polarized dissociation light. They are equal to the maximum possible values of the corresponding state multipoles A_{K0}^{mol}. The anisotropy parameters in eqs 28 and 29 are associated with linearly polarized dissociation light. If $\beta = -1$ or $\beta = 2$, the corresponding A_{20}^{mol}, A_{22}^{mol}, and A_{32}^{mol} do not depend on the angle θ.[10]

The parameter $\mathrm{Re}[\mathbf{a}_1^{(1)}]$ in eq 20 is only associated with the circularly polarized components of the dissociation light. This parameter divided by the coefficient $-\sqrt{2(1+\beta)(2-\beta)}$ is equal to the maximum value of the molecular frame state multipole $A_{11}^{\mathrm{mol}}(\beta,\theta_c)$ at $\beta = 0$ and $\theta_c = \pi/2$.

Appendix B: Speed-Dependent Model

Assuming that the two areas of nonadiabatic behavior have no overlap with each other and that the nonadiabatic interaction occurs between only two of the states within each area, the following speed-depended model can be suggested. The expansion of the Hund's case (a) molecular wave function over the product of the free atom wave function can still be written as in eq 25, however the expansion coefficients $K_{j_A\Omega_A j_B\Omega_B}(S,\Sigma,\Lambda)$ can be presented as

$$\tilde{K}_{(1/2)(1/2)(1/2)(1/2)}(A^1\Pi_1) = \sqrt{P_1} \tag{31}$$

$$\tilde{K}_{(1/2)(1/2)(3/2)(1/2)}(A^1\Pi_1) = \sqrt{(1-P_1)P_2} \tag{32}$$

and

$$\tilde{K}_{(1/2)-(1/2)(3/2)(3/2)}(A^1\Pi_1) = \sqrt{(1-P_1)(1-P_2)} \tag{33}$$

where P_1 and P_2 are probabilities of the nonadiabatic transition between the $A^1\Pi_1$ state and the $t^3\Sigma_1$ and $a^3\Pi_1$ states, respectively. The H atom (H electron) spin polarization can then readily be determined as

$$P_e^{\max} = P_1 + (1-P_1)P_2 - (1-P_1)(1-P_2) \tag{34}$$

The probability P_1 can be calculated using the known analytical solution of a model two-level problem. According to the exponential two-state model,[73] the difference between two adiabatic potential curves a and b is presented as function of the internuclear distance R as

$$\Delta U_{a,b} = \Delta\epsilon[1 - 2\cos\tilde{\theta}e^{-\alpha(R-R_p)} + e^{-2\alpha(R-R_p)}]^{1/2} \tag{35}$$

The kinetic energy operator which is responsible for the nonadiabatic interaction in the adiabatic representation is

$$(\partial/\partial R)_{a,b} = \frac{\alpha\sin\tilde{\theta}e^{-\alpha(R-R_p)}}{1 - 2\cos\tilde{\theta}e^{-\alpha(R-R_p)} + e^{-2\alpha(R-R_p)}} \tag{36}$$

Equations 35 and 36 contain four fitting parameters: $\Delta\epsilon$, $\tilde{\theta}$, α, and R_p.

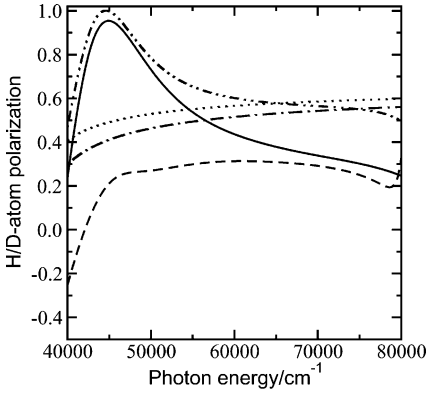

Figure 7. H atom polarization as a function of photon energy for the photodissociation of HCl and DCl initially in their ground, $v = 0$, vibrational states as computed exactly (solid and dashed lines, respectively) and using the speed-dependent model of Appendix B (dotted and dash−dot lines, respectively). The H-atom polarization determined using the speed-dependent model with an "exact" value of P_2 (dot−dot−dash line); see text for details.

Assuming uniform nuclei movement, the difference potential in eq 35 and the interaction operator in eq 36 result in the transition probability P

$$P_1 = e^{-\pi\xi_p}\frac{\sinh(\pi\xi - \pi\xi_p)}{\sinh(\pi\xi)} \qquad (37)$$

where ξ and ξ_p are the Massey parameter and the Massey parameter in the transition area, respectively. They are defined as[73] $\xi = \Delta\epsilon/(\alpha v)$ and $\xi_p = \xi(1 - \cos\tilde{\theta})/2$, where v is the fragment relative velocity, while $\Delta\epsilon$, α, and $\tilde{\theta}$ are the parameters of the model.

In the first nonadiabatic area at $3.5 \le R \le 5.5$ bohr, the potential energy difference (eq 35) was associated with the $t^3\Sigma_1$ and $A^1\Pi_1$ potential curves. Using the potential curve data from ref 25, we obtained the following values of the fitting parameters for the nonadiabatic area 1: $\Delta\epsilon = 0.00393$ au, $\cos\tilde{\theta} = 0.377$, $\alpha = 2.020$, and $R_p = 4.36$ bohr. These values were used for calculating the two Massey parameters and the nonadiabatic transition probability P_1 with respect to eq 38.

Assuming strong nonadiabatic interaction between the $A^1\Pi_1$ and the $a^3\Pi_1$ states in the second area, we used the statistical model and set $P_2 = 1/2$.

The polarization degree P_e^{max} of the H and D fragments resulting from eq 35 is presented in Figure 7 along with the results of the exact dynamics calculation. Comparison of the data in Figure 7 shows that the separate nonadiabatic area model qualitatively correctly predicts high polarization of the H fragments in the entire energy range and the polarization decrease at low energy. However, this model does not predict high energy decrease of the fragment polarization which is probably due to interaction between all three quantum states at large distances (from $R \simeq 5$ bohr to $R \simeq 8$ bohr). Also, the model does not agree quantitatively with the results of exact calculations at low energy by not reproducing the low energy maximum in the polarization for HCl and by giving a noticeably larger polarization for DCl. The failure is due to our simplistic statistical assumption of $P_2 = 1/2$ used for the large distance nonadiabatic area; the failure of this assumption was readily verified by computing P_2 utilizing the model developed in ref 21 for HF. Using the "exact" value of P_2 rather than the constant value of one-half, we can correct the determination of P_e^{max}. The corrected result for HCl is shown in Figure 7 and as one can see the energy dependence is much more faithfully reproduced. The problem is that one requires an exact determination of P_2 in order to obtain this result.

So, qualitatively the simple speed-dependent model reproduces some of the energy dependence of the exact results but clearly further developments are needed to provide quantitative (or even qualitative across the entire energy range) predictions without resorting to input from exact dynamical calculations.

Acknowledgment. A.B. thanks Dr. T. P. Rakitzis (University of Crete) for useful discussions. G.G.B.K. thanks EPSRC for financial support. The authors thank Prof. J. A. Beswick (Université Paul Sabatier) for his contributions to the theoretical formalism underpinning this work and for useful discussions.

References and Notes

(1) van Brunt, R. J.; Zare, R. N. *J. Chem. Phys.* **1968**, *48*, 4304.
(2) Jonah, C.; Chandra, P.; Bersohn, R. *J. Chem. Phys.* **1971**, *55*, 1903.
(3) Solomon, J.; Jonah, C.; Chandra, P.; Bersohn, R. *J. Chem. Phys.* **1971**, *55*, 1908.
(4) Siebbeles, L. D. A.; Glass-Maujean, M.; Vasyutinskii, O. S.; Beswick, J. A.; Roncero, O. *J. Chem. Phys.* **1994**, *100*, 3610.
(5) Rakitzis, T. P.; Zare, R. N. *J. Chem. Phys.* **1999**, *110*, 3341.
(6) Rakitzis, T. P.; Kandel, S. A.; Alexander, A. J.; Kim, Z. H.; Zare, R. N. *J. Chem. Phys.* **1999**, *110*, 3351.
(7) Picheyev, B. V.; Smolin, A. G.; Vasyutinskii, O. S. *J. Phys. Chem. A* **1997**, *101*, 7614.
(8) Wouters, E. R.; Ahmed, M.; Peterska, D. S.; Bracker, A. S.; Suits, A. G.; Vasyutinskii, O. S. In *Imaging in Chemical Dynamics*; Suits, A. G., Continetti, R. E., Eds.; American Chemical Society: Washington, DC, 2000.
(9) Rakitzis, T. P.; Kitsopoulos, T. N. *J. Chem. Phys.* **2002**, *116*, 9228.
(10) Bracker, A. S.; Wouters, E. R.; Suits, A. G.; Vasyutinskii, O. S. *J. Chem. Phys.* **1999**, *110*, 6749.
(11) Mo, Y.; Katayanagi, H.; Heaven, M. C.; Suzuki, M. C. *Phys. Rev. Lett.* **1996**, *77*, 830.
(12) Eppink, A. T. J. B.; Parker, D. H.; Janssen, M. H. M.; Buijsse, B.; van der Zande, W. J. *J. Chem. Phys.* **1998**, *108*, 1305.
(13) Wang, Y. F.; Loock, H. P.; Cao, J.; Qian, C. X. W. *J. Chem. Phys.* **1995**, *102*, 808.
(14) North, S. W.; Zheng, X. S.; Fei, R.; Hall, G. E. *J. Chem. Phys.* **1996**, *104*, 2129.
(15) Costen, M. L.; North, S. W.; Hall, G. E. *J. Chem. Phys.* **1999**, *111*, 6735.
(16) Bass, M. J.; Brouard, M.; Clark, A. P.; Vallance, C.; Martinez-Haya, B. *Phys. Chem. Chem. Phys.* **2003**, *5*, 856.
(17) Bracker, A. S.; Wouters, E. R.; Suits, A. G.; Lee, Y. T.; Vasyutinskii, O. S. *Phys. Rev. Lett.* **1998**, *80*, 1626.
(18) Alexander, A. J.; Kim, Z. H.; Kandel, S. A.; Zare, R. N.; Asano, Y.; Yabushita, S. *J. Chem. Phys.* **2000**, *113*, 9022.
(19) Wouters, E. R.; Beckert, M.; Russell, L. J.; Rosser, K. N.; Orr-Ewing, A. J.; Ashfold, M. N. R.; Vasyutinskii, O. S. *J. Chem. Phys.* **2002**, *117*, 2087.
(20) Rakitzis, T. P.; Samrtzis, P. C.; Toomes, R. L.; Tsigaridas, L.; Coriou, M.; Chestakov, D.; Eppink, A. T. J. B.; Parker, D. H.; Kitsopoulos, T. N. *Chem. Phys. Lett.* **2002**, *364*, 115.
(21) Balint-Kurti, G. G.; Orr-Ewing, A. J.; Beswick, J. A.; Brown, A.; Vasyutinskii, O. S. *J. Chem. Phys.* **2002**, *116*, 10 760.
(22) Asano, Y.; Yabushita, S. *J. Phys. Chem. A* **2001**, *105*, 9873.
(23) Rakitzis, T. P.; Samartzis, P. C.; Toomes, R. L.; Kitsopoulos, T. N.; Brown, A.; Balint-Kurti, G. G.; Vasyutinskii, O. S.; Beswick, J. A. *Science* **2003**, *300*, 1936.
(24) van Vroohoven, M. C. G. N.; Groenenboom, G. C. *J. Chem. Phys.* **2002**, *116*, 1965.
(25) Alexander, M. H.; Pouilly, B.; Duhoo, T. *J. Chem. Phys.* **1993**, *99*, 1752.
(26) Lambert, H. M.; Dagdigian, P. J.; Alexander, M. H. *J. Chem. Phys.* **1998**, *108*, 4460.
(27) Cheng, B. M.; Chung, C. Y.; Bahou, M.; Lee, Y. P.; Lee, L. C. *J. Chem. Phys.* **2002**, *117*, 4293.
(28) Regan, P. M.; Ascenzi, D.; Brown, A.; Balint-Kurti, G. G.; Orr-Ewing, A. J. *J. Chem. Phys.* **2000**, *112*, 10 259.
(29) Regan, P. M.; Langford, S. R.; Ascenzi, D.; Cook, P. A.; Orr-Ewing, A. J.; Ashfold, M. N. R. *Phys. Chem. Chem. Phys.* **1999**, *1*, 3247.
(30) Ascenzi, D.; Regan, P. M.; Orr-Ewing, A. J. *Chem. Phys. Lett.* **1999**, *310*, 477.
(31) Jr., I. B.; Jalbert, G.; Bielschowsky, C. E. *J. Phys. B: At. Mol. Opt. Phys.* **1998**, *31*, 3703.
(32) Zhang, J.; Dulligan, M.; Wittig, C. *J. Chem. Phys.* **1997**, *107*, 1403.
(33) Tonokura, K.; Matsumi, Y.; Kawasaki, M.; Tasaki, S.; Bersohn, R. *J. Chem. Phys.* **1992**, *97*, 8210.

(34) Lee, S.; Jung, K. H. *J. Chem. Phys.* **2000**, *112*, 2810.
(35) Li, Y.; Bludsky, O.; Hirsch, G.; Buenker, R. J. *J. Chem. Phys.* **2000**, *112*, 260.
(36) Duhoo, T.; Pouilly, B. *J. Chem. Phys.* **1995**, *103*, 182.
(37) Gersonde, I. H.; Henning, S.; Gabriel, H. *J. Chem. Phys.* **1994**, *101*, 9558.
(38) Givertz, S. C.; Balint-Kurti, G. G. *J. Chem. Soc. Far. Trans.* **1986**, *82*, 1231.
(39) van Dishoeck, E.; van Hemert, M.; Dalgarno, A. *J. Chem. Phys.* **1982**, *77*, 3693.
(40) Balint-Kurti, G. G.; Dixon, R. N.; Marston, C. C. *J. Chem. Soc. Far. Trans.* **1990**, *86*, 1741.
(41) Brown, A.; Balint-Kurti, G. G. *J. Chem. Phys.* **2001**, *113*, 1870.
(42) Balint-Kurti, G. G. *Adv. Chem. Phys.* **2003**, *128*, 249.
(43) Adams, G. F.; Chalabowski, C. F. *J. Phys. Chem.* **1994**, *98*, 5878.
(44) Stevens, W. J.; Krauss, M. *J. Chem. Phys.* **1982**, *77*, 1368.
(45) Bettendorf, M.; Peyerimhoff, S. D.; Buenker, R. J. *Chem. Phys.* **1982**, *66*, 261.
(46) Hirst, D. M.; Guest, M. F. *Mol. Phys.* **1980**, *41*, 1483.
(47) Moore, C. E. *Atomic Energy Levels*; U.S. Government Printing Office: Washington, D. C., 1971.
(48) Brown, A.; Balint-Kurti, G. G. *J. Chem. Phys.* **2001**, *113*, 1879.
(49) Givertz, S. Thesis, University of Bristol, 1982.
(50) Balint-Kurti, G. G.; Dixon, R. N.; Marston, C. C. *Int. Rev. Phys. Chem.* **1992**, *11*, 317.
(51) Heller, E. J. *J. Chem. Phys.* **1978**, *68*, 2066.
(52) Heller, E. J. *J. Chem. Phys.* **1978**, *68*, 3891.
(53) Heller, E. J. *Acc. Chem. Res.* **1981**, *14*, 368.
(54) Marston, C. C.; Balint-Kurti, G. G. *J. Chem. Phys.* **1989**, *91*, 3571.
(55) Balint-Kurti, G. G.; Ward, C. L.; Marston, C. C. *Comput. Phys. Comm.* **1991**, *67*, 285.
(56) Balint-Kurti, G. G.; Shapiro, M. *Chem. Phys.* **1981**, *61*, 137.
(57) Balint-Kurti, G. G.; Shapiro, M.. In *Photodissociation and Photoionization*; Lawley, K. P., Ed.; John Wiley & Sons: New York, 1985.
(58) Zare, R. N. *Angular Momentum*; World Scientific: New York, 1988.
(59) Edmonds, A. R. *Angular Momentum in Quantum Mechanics;* Princeton University Press: Princeton, 1960.
(60) Blum, K. *Density Matrix Theory and Applications*; Plenum: New York, 2nd ed.; 1990.
(61) Kupriayanov, D. V.; Vasyutinskii, O. S. *Chem. Phys.* **1993**, *171*, 25.
(62) Zare, R. N. *Mol. Photochem.* **1972**, *4*, 1.
(63) Rakitzis, T. P.; Hall, G.; Costen, M. L.; Zare, R. N. *J. Chem. Phys.* **1999**, *111*, 8751.
(64) Rakitzis, T. P., personal communication.
(65) Rottke, H.; Zacharias, H. *Phys. Rev. A* **1986**, *33*, 736.
(66) Happer, W. H. *Rev. Mod. Phys.* **1972**, *44*, 169.
(67) Matsumi, Y.; Tonokura, K.; Kawasaki, M.; Ibuki, T. *J. Chem. Phys.* **1990**, *93*, 7981.
(68) Singer, S. J.; Freed, K. F. *Adv. Chem. Phys.* **1985**, *61*, 1.
(69) Brown, A.; Balint-Kurti, G. G., unpublished.
(70) Pouilly, B.; Monnerville, M. *Chem. Phys.* **1998**, *238*, 437.
(71) Kalyanaraman, C.; Sathyamurthy, N. *Chem. Phys. Lett.* **1993**, *209*, 52.
(72) Alekseyev, A. B.; Liebermann, H. P.; Kokh, D. B.; Buenker, R. J. *J. Chem. Phys.* **2000**, *113*, 6174.
(73) Nikitin, E. E.; Umanskii, S. Y. *Theory of Slow Atomic Collisions*; Springer: Berlin, 1984.